Analytical Methods

DOI: 10.1002/anie.201205436

Observation of Subcellular Metabolite Gradients in Single Cells by Laser Ablation Electrospray Ionization Mass Spectrometry**

*Jessica A. Stolee, Bindesh Shrestha, Getachew Mengistu, and Akos Vertes**

In recent years an increasing number of methods have been exploited for the proteomic[1–4] and metabolomic[5–8] analysis of single cells and have provided new insight into cellular subtypes. Local analysis on a subcellular level, however, requires new approaches. Heterogeneity of metabolite distributions within a cell is attributed to functional organization, compartmentalization into organelles, macromolecular crowding, and metabolite channeling as a result of the colocalization of enzymes.[9,10] This heterogeneity results in metabolite gradients within a cell and compartmentalization of metabolites in particular organelles.[11] The intracellular production, reaction, and redistribution of metabolites do not always follow the kinetics established in vitro at low concentrations.[12] Subcellular trafficking between compartments often relies on active transport facilitated by transporter proteins.[13,14] For example, secondary metabolites can accumulate in the vacuole by the help of ABC transporters.[15–17] Determining the subcellular distributions of metabolites is challenging because of their high diffusion rates and rapid turnover.

Most techniques for the subcellular analysis of eukaryotic cells rely on the isolation of organelles by nonaqueous fractionation and require extensive sample preparation prior to chemical analysis.[18] By using tagging or labeling techniques, the distribution of some preselected metabolites can be followed by fluorescence resonance energy transfer.[19] More recently, cell-membrane lipid distributions have been analyzed by secondary ion mass spectrometry (SIMS)[20,21] and selected metabolite levels have been determined in the cytoplasm, cytosolic lipid droplets, vacuole, granule, and nucleus by nano-electrospray ionization mass spectrometry.[22–25] There are, however, few label-free multispecies methods that capture the spatial localization of diverse metabolites within a cell.

Femtosecond laser pulses have been used for disrupting and dissecting subcellular organelles, such as mitochondria and nuclei, in living mammalian cells.[26–28] This nanosurgery technique, however, is typically performed without opening the cell, therefore the resulting ablation products are not available for analysis.[29–31] In laser ablation electrospray ionization (LAESI) of biological samples, a mid-infrared laser generates a plume in the surrounding environment by bursting the cells open. The ejected material is ionized by an electrospray and analyzed by a mass spectrometer.[32–35] The ablation and analysis of metabolites in single cells has been achieved by delivering the mid-IR laser pulses with an etched optical fiber for LAESI analysis.[8,36,37] Herein, we report the in situ chemical analysis of metabolites localized in subcellular compartments by the combination of microdissection and LAESI–MS. We demonstrate the direct multispecies molecular analysis of subcellular compartments by this ambient ionization method. Large metabolite gradients between the cytoplasm and nucleus of *Allium cepa* epidermal cells are observed using this novel technique.

The schematic in Figure 1 shows the essential features of the experimental setup labeled with the critical dimensions. Epidermal cells from the *A. cepa* bulb were used as a model system in the form of an intact monolayer. The cell nuclei were visible without histological staining (see Figure 2a). A cellular monolayer of epidermal tissue was mounted onto a glass slide, and a micromanipulator equipped with a microdissection needle with a tip diameter of approximately 1 μm was used for the microdissection. The tip was lowered to the cell wall to pierce and cut it along the inner edge, and peel it back to expose the cytoplasm and the organelles. The

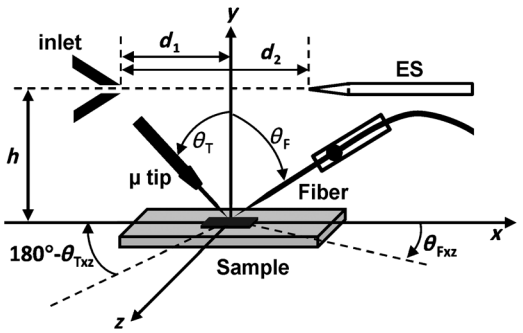

Figure 1. Schematic of the subcellular LAESI and microdissection setup. The sample is mounted on an *x*-*y*-*z* translation stage. Microdissection is performed by a sharp tungsten needle (μ tip) followed by mid-IR laser ablation of the subcellular compartment using an etched optical fiber. The mass spectrometer inlet and electrospray emitter (ES) are on the same axis at a distance of $d_2 = 12$ mm. The sample is positioned at $h = 15$ mm below this axis. The projection of the point of dissection to this axis is at $d_1 = 7$ mm away from the inlet. The polar angles of the microdissection tip and the fiber are $\theta_T = 45–60°$ and $\theta_F = 45–60°$, respectively. The corresponding azimuthal angles are $\theta_{Txz} = 120–135°$ and $\theta_{Fxz} = 45–60°$, respectively.

[*] J. A. Stolee, Dr. B. Shrestha, G. Mengistu, Prof. A. Vertes
Department of Chemistry, The George Washington University
Washington, DC 20052 (USA)
E-mail: vertes@gwu.edu
Homepage: http://www.gwu.edu/~vertes

[**] Financial support from the U.S. National Science Foundation (Grant CHE-1152302), and the U.S. Department of Energy Grant DEFG02-01ER15129) is acknowledged. Infrared Fiber systems, Silver Spring, MD, generously provided the GeO_2-based glass fibers.

Supporting information for this article is available on the WWW under http://dx.doi.org/10.1002/anie.201205436.

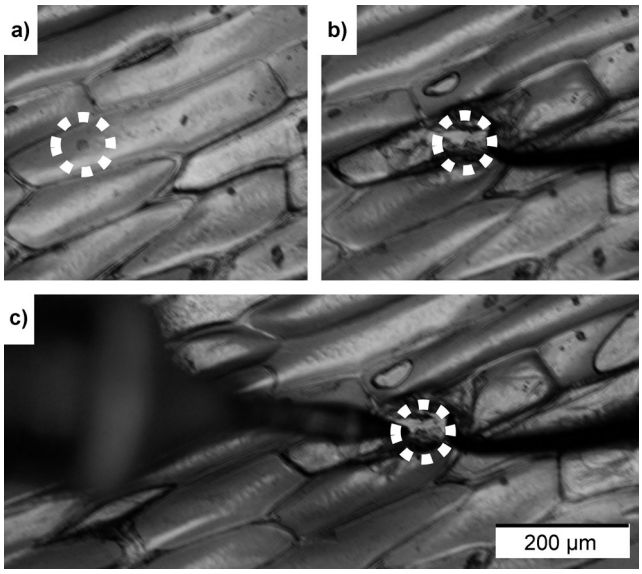

Figure 2. Microscope images of *A. cepa* epidermal cells show: a) the intact cells and the targeted nucleus prior to microdissection in the dotted white circle; b) the microdissection tip as it peels back the cell wall exposing the nucleus; and c) the etched optical fiber tip as it is brought adjacent to the nucleus prior to ablation.

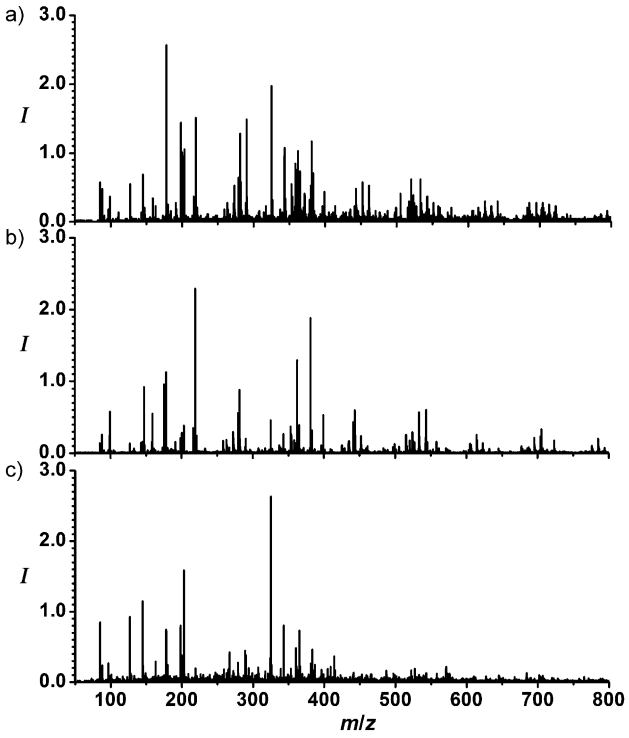

Figure 3. Mass spectra obtained from: a) a single intact *A. cepa* epidermal cell; b) the cytoplasm of a microdissected cell; and c) the nucleus of a microdissected cell. Distinct differences can be observed between the spectra of the cytoplasm and the nucleus samples.

neighboring cells were not disrupted during the microdissection, and the nucleus remained intact (see Figure 2b). Immediately after the microdissection, a germanium oxide based optical fiber with a tip diameter of approximately 15 µm was brought adjacent to the nucleus to deliver mid-IR laser pulses at a wavelength of 2940 nm (Figure 2c). The laser energy emitted at the fiber tip decayed within a distance comparable to the tip diameter. In aqueous environment this energy is reduced by the strong absorption of the 2940 nm radiation. The microdissection and ablation were visualized from the top with a long-distance microscope to pinpoint the targeted cellular component. A side-view microscope was used to monitor the distance between the cell surface and the needle or the fiber. The ablation products were ionized by charged droplets from an electrospray emitter that was on the same axis as the inlet of a mass spectrometer.

To obtain the spectra corresponding to the entire cell, initially intact epidermal cells were ablated and analyzed (see Figure 3a). Subsequently, microdissection was performed on an epidermal cell to expose the subcellular components. When the cytoplasm away from the nucleus was targeted with the fiber tip, LAESI–MS yielded a feature-rich spectrum (see Figure 3b), with many of the same peaks that were detected for the intact single cell. Mass spectra from the cell cytoplasm contained peaks primarily corresponding to singly protonated molecules, quasimolecular (sodium or potassium adducts) ions, and a few dimers. Tentative peak assignments were based on accurate mass measurements, information found in databases, such as the Plant Metabolic Network database (http://plantcyc.org/), and the related literature, as well as previous experimental results, including tandem MS measurements, from LAESI analysis of *A. cepa* cells.[36] See Table S1 in the Supporting Information for the tentative identification of selected peaks. For example, highly abundant hexose, alliin, and oligosaccharides were among the putatively assigned metabolites detected in the cell cytoplasm.

Selective ablation of the nuclear region was possible because the sharpened tip of the optical fiber was comparable in size to the approximately 20 µm diameter of the cell nucleus. A significant number of peaks, corresponding to over thirty metabolites, were observed in the spectrum obtained from the nucleus (Figure 3c). As a result of the lower volume of material in a nucleus than that of the cytoplasm or a single cell, the mass spectra obtained from it exhibited lower signal intensities. As expected, some common metabolites between the nucleus and cytoplasm were detected because some cross-contamination by the cytoplasm surrounding the nucleus is inevitable. However, the relative intensities of metabolites varied. For example, the peak at m/z 219 (potassium adduct of hexose) was one of the strongest peaks in the spectra obtained from the cytoplasm and, in most cases, had a relative intensity of less than 40% in spectra from the nucleus. Comparisons between the normalized intensities of ions in the nucleus and cytoplasm spectra can be found in Figure S1 in the Supporting Information. The ratios of the peak intensities between the nucleus and cytoplasm spectra are also noted in Table S1.

To identify metabolites with strong variance between the nucleus and the cytoplasm, multivariate statistical analysis, in particular orthogonal projections to latent structures discriminant analysis (OPLS-DA), was performed on the mass spectra. This method enabled us to separate predictive components, that is, those responsible for the differences between the two organelles, from nonpredictive variations, that is, those describing the differences between one nucleus

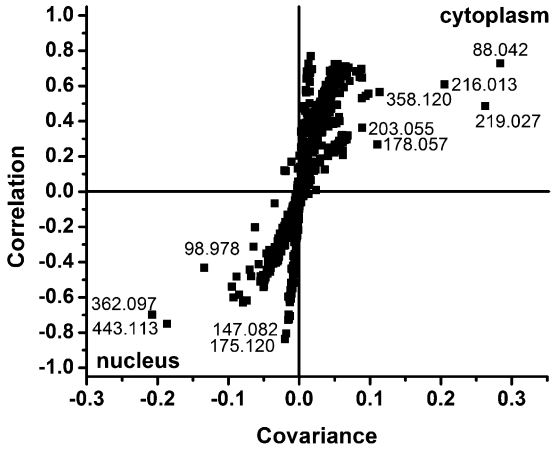

Figure 4. Metabolites that account for most of the variance in the spectra between the cytoplasm and the nucleus are found by the S plot. Peaks with high covariance are correlated either to the cytoplasm (top right) or to the nucleus (bottom left). See Table S2 in the Supporting Information for the putative identification of these metabolites.

and another. The resulting S plot, shown in Figure 4, highlights the metabolites with high correlation and covariance. For example, metabolites that are more specific to the cytoplasm, such as hexose (*m*/*z* 203 and 219) and alliin (*m*/*z* 178), are in upper right corner, whereas those that are more characteristic of the nucleus, such as arginine (*m*/*z* 175) and glutamine (*m*/*z* 147) are in the lower left corner. The points located near the center represent metabolites that are not statistically different in the two regions. The putative assignments of the statistically different metabolites (labeled with their *m*/*z* values) are listed in Table S2 in the Supporting Information.

These results demonstrate that hexose and some of the secondary metabolites, for example, alliin, primarily accumulate in the cytoplasm. Indeed, hexose is known to be more abundant in the vacuoles, and it has been suggested that this is the result of an active uptake mechanism.[38,39] In contrast, some amino acids were more readily detected in the nuclei. Although there have been very few studies on the localization of metabolites in plant nuclei, other small metabolites, such as flavonoids, have been found to be localized in them.[40,41] Furthermore, the enzyme involved in the metabolism of arginine, that is, arginine decarboxylase, has been found to be localized to the nuclei of nonphotosynthetic tissues; this finding may suggest the presence of arginine in the studied nuclei.[42] As the compartmentalization of metabolites in the nucleus is relatively unexplored, questions remain as to whether these metabolites are locally produced, consumed, or actively transported to them.

To validate our findings on the large metabolite gradients between the nucleus and the cytoplasm with independent methods, additional experiments were performed. A cationic dye, toluidine blue, with an affinity to the nucleus was introduced to stain the sample. Optical microscope images confirmed that the dye molecules preferentially localized in the nuclei. In situ analysis of dissected stained cells by LAESI also identified significantly higher abundance of the dye molecules in the nucleus than in the cytoplasm, resulting in an intensity ratio of $I_{nuc/cyt} = 3.0$. Further confirmation was obtained by separately extracting the nucleus and the cytoplasm from the cells stained by methylene blue using a nanoelectrospray emitter.[43] Images of a cell before and after the extraction of the nucleus confirm its successful removal with minimal damage to the cell (see Figure S2a and S2b in the Supporting Information). The captured nucleus is clearly visible at the tip of the emitter (see the inset in Figure S2c in the Supporting Information). The mass spectra of the nucleus and cytoplasm samples were obtained by using direct electrospray ionization; in the spectrum of the nucleus sample significantly stronger peaks corresponding to the methylene blue molecular ion are seen (see Figure S2c and the experimental details in the Supporting Information). Indeed, multiple experiments show an intensity ratio of $I_{nuc/cyt} = 2.5$. Thus both microdissection combined with LAESI and organelle extraction followed by electrospray ionization indicate that for staining agents our results are consistent with the optically discernible gradient. It is therefore expected that the abundance differences observed for metabolites also reflect existing gradients.

In summary, we have demonstrated in situ ambient analysis of a large number of metabolites from subcellular regions by performing cell microdissection, selective ablation, and LAESI mass spectrometry. This method provides insight into the distribution of metabolites on a subcellular level with minimal change to the integrity of the compartments. The results show that the metabolic makeup of the nucleus and cytoplasm are significantly different. The often large concentration gradients may result from the compartmentalization of metabolites, metabolic channeling, and the active uptake of metabolites for, for example, energy storage or detoxification. Furthermore, local production or consumption of metabolites may also contribute to the differences in the metabolite composition. Additional studies may shed light on the different mechanisms that result in these metabolite gradients.

Although we used relatively large cells, this technique can be extended to explore subcellular heterogeneity in smaller cells. The current analytical challenge lies in the sensitivity of the mass spectrometer. As single cell technologies advance, we expect fast developments in subcellular analysis. Microdissection combined with LAESI mass spectrometry has the potential to address important biological questions arising from subcellular heterogeneity and give insight into the subcellular variations of metabolic pathways affected by diseases and drug delivery.

Received: July 10, 2012
Published online: September 5, 2012

Keywords: analytical methods · electrospray ionization · mass spectrometry · metabolomics · single-cell analysis

[1] S. C. Bendall, E. F. Simonds, P. Qiu, E. A. D. Amir, P. O. Krutzik, R. Finck, R. V. Bruggner, R. Melamed, A. Trejo, O. I. Ornatsky,

R. S. Balderas, S. K. Plevritis, K. Sachs, D. Pe'er, S. D. Tanner, G. P. Nolan, *Science* **2011**, *332*, 687 – 696.
[2] M. L. Kovarik, N. L. Allbritton, *Trends Biotechnol.* **2011**, *29*, 222 – 230.
[3] A. Schmid, H. Kortmann, P. S. Dittrich, L. M. Blank, *Curr. Opin. Biotechnol.* **2010**, *21*, 12 – 20.
[4] Q. H. Shi, L. D. Qin, W. Wei, F. Geng, R. Fan, Y. S. Shin, D. L. Guo, L. Hood, P. S. Mischel, J. R. Heath, *Proc. Natl. Acad. Sci. USA* **2012**, *109*, 419 – 424.
[5] M. Heinemann, R. Zenobi, *Curr. Opin. Biotechnol.* **2011**, *22*, 26 – 31.
[6] A. Oikawa, K. Saito, *Plant J.* **2012**, *70*, 30 – 38.
[7] S. S. Rubakhin, E. V. Romanova, P. Nemes, J. V. Sweedler, *Nat. Methods* **2011**, *8*, S20 – S29.
[8] B. Shrestha, J. M. Patt, A. Vertes, *Anal. Chem.* **2011**, *83*, 2947 – 2955.
[9] J. M. Rohwer, P. W. Postma, B. N. Kholodenko, H. V. Westerhoff, *Proc. Natl. Acad. Sci. USA* **1998**, *95*, 10547 – 10552.
[10] J. Ovádi, V. Saks, *Mol. Cell. Biochem.* **2004**, *256*, 5 – 12.
[11] J. Yon-Kahn, G. Hervé, G. Hervé, *Molecular and Cellular Enzymology*, Springer, Berlin, **2010**, pp. 727 – 739.
[12] C. K. Choi, J. D. Fowlkes, S. T. Retterer, P. Siuti, S. Iyer, M. J. Doktycz, *ACS Nano* **2010**, *4*, 3345 – 3355.
[13] M. Maeshima, *Annu. Rev. Plant Physiol. Plant Mol. Biol.* **2001**, *52*, 469 – 497.
[14] N. C. Danbolt, *Prog. Neurobiol.* **2001**, *65*, 1 – 105.
[15] P. J. Verrier, D. Bird, B. Buria, E. Dassa, C. Forestier, M. Geisler, M. Klein, U. Kolukisaoglu, Y. Lee, E. Martinoia, A. Murphy, P. A. Rea, L. Samuels, B. Schulz, E. P. Spalding, K. Yazaki, F. L. Theodoulou, *Trends Plant Sci.* **2008**, *13*, 151 – 159.
[16] E. Martinoia, M. Klein, M. Geisler, L. Bovet, C. Forestier, U. Kolukisaoglu, B. Muller-Rober, B. Schulz, *Planta* **2002**, *214*, 345 – 355.
[17] E. Martinoia, M. Maeshima, H. E. Neuhaus, *J. Exp. Bot.* **2007**, *58*, 83 – 102.
[18] S. Krueger, P. Giavalisco, L. Krall, M. C. Steinhauser, D. Bussis, B. Usadel, U. I. Flugge, A. R. Fernie, L. Willmitzer, D. Steinhauser, *Plos One* **2011**, *6*, e17806.
[19] M. Fehr, W. B. Frommer, S. Lalonde, *Proc. Natl. Acad. Sci. USA* **2002**, *99*, 9846 – 9851.
[20] S. G. Ostrowski, M. E. Kurczy, T. P. Roddy, N. Winograd, A. G. Ewing, *Anal. Chem.* **2007**, *79*, 3554 – 3560.
[21] S. G. Ostrowski, C. T. Van Bell, N. Winograd, A. G. Ewing, *Science* **2004**, *305*, 71 – 73.
[22] S. Date, H. Mizuno, N. Tsuyama, T. Harada, T. Masujima, *Anal. Sci.* **2012**, *28*, 201 – 203.
[23] T. Masujima, *Anal. Sci.* **2009**, *25*, 953 – 960.
[24] H. Mizuno, N. Tsuyama, T. Harada, T. Masujima, *J. Mass Spectrom.* **2008**, *43*, 1692 – 1700.
[25] P. J. Horn, N. R. Ledbetter, C. N. James, W. D. Hoffman, C. R. Case, G. F. Verbeck, K. D. Chapman, *J. Biol. Chem.* **2011**, *286*, 3298 – 3306.
[26] T. Shimada, W. Watanabe, S. Matsunaga, T. Higashi, H. Ishii, K. Fukui, K. Isobe, K. Itoh, *Opt. Express* **2005**, *13*, 9869 – 9880.
[27] N. Shen, D. Datta, C. Schaffer, P. LeDuc, D. Ingber, E. Mazur, *Mech. Chem. Biosyst.* **2005**, *2*, 17 – 25.
[28] K. Konig, I. Riemann, P. Fischer, K.-J. Halbhuber, *Cell. Mol. Biol.* **1999**, *45*, 195 – 202.
[29] K. Kuetemeyer, R. Rezgui, H. Lubatschowski, A. Heisterkamp, *Biomed. Opt. Express* **2010**, *1*, 587 – 597.
[30] P. Ronchi, S. Terjung, R. Pepperkok, *Biol. Chem.* **2012**, *393*, 235 – 248.
[31] A. Vogel, J. Noack, G. Huttman, G. Paltauf, *Appl. Phys. B* **2005**, *81*, 1015 – 1047.
[32] P. Nemes, A. Vertes, *Anal. Chem.* **2007**, *79*, 8098 – 8106.
[33] P. Nemes, A. A. Barton, Y. Li, A. Vertes, *Anal. Chem.* **2008**, *80*, 4575 – 4582.
[34] P. Nemes, A. A. Barton, A. Vertes, *Anal. Chem.* **2009**, *81*, 6668 – 6675.
[35] P. Nemes, A. S. Woods, A. Vertes, *Anal. Chem.* **2010**, *82*, 982 – 988.
[36] B. Shrestha, A. Vertes, *Anal. Chem.* **2009**, *81*, 8265 – 8271.
[37] B. Shrestha, P. Nemes, A. Vertes, *Appl. Phys. A* **2010**, *101*, 121 – 126.
[38] D. Heineke, K. Wildenberger, U. Sonnewald, L. Willmitzer, H. W. Heldt, *Planta* **1994**, *194*, 29 – 33.
[39] A. Endler, S. Meyer, S. Schelbert, T. Schneider, W. Weschke, S. W. Peters, F. Keller, S. Baginsky, E. Martinoia, U. G. Schmidt, *Plant Physiol.* **2006**, *141*, 196 – 207.
[40] W. Feucht, D. Treutter, J. Polster, *Plant Cell Rep.* **2004**, *22*, 430 – 436.
[41] J. Polster, H. Dithmar, R. Burgemeister, G. Friedemann, W. Feucht, *Physiol. Plant.* **2006**, *128*, 163 – 174.
[42] C. Bortolotti, A. Cordeiro, R. Alcazar, A. Borrell, F. A. Culianez-Macia, A. F. Tiburcio, T. Altabella, *Physiol. Plant.* **2004**, *120*, 84 – 92.
[43] N. Tsuyama, H. Mizuno, E. Tokunaga, T. Masujima, *Anal. Sci.* **2008**, *24*, 559 – 561.

